HHS Public Access

Author manuscript

Bone. Author manuscript; available in PMC 2023 June 01.

Published in final edited form as:

Bone. 2022 June ; 159: 116391. doi:10.1016/j.bone.2022.116391.

GIRK3 deletion facilitates kappa opioid signaling in chondrocytes, delays vascularization and promotes bone lengthening in mice

Earnest L. Taylor[1,2,§], **Samantha R. Weaver**[1,§], **Ian M. Lorang**[1,3], **Katherine M. Arnold**[4], **Elizabeth W. Bradley**[1,5], **Ezequiel Marron Fernandez de Velasco**[6], **Kevin Wickman**[6], **Jennifer J. Westendorf**[1,7]

[1]Department of Orthopedic Surgery, Mayo Clinic, Rochester, MN

[2]Department of Cell Biology, University of North Carolina, NC

[3]University of Washington School of Medicine, Seattle, Washington

[4]Mayo Clinic Graduate School of Biomedical Sciences, Mayo Clinic, Rochester, MN

[5]Department of Orthopedic Surgery, University of Minnesota, Minneapolis, MN

[6]Department of Pharmacology, University of Minnesota, Minneapolis, MN

[7]Department of Biochemistry and Molecular Biology, Mayo Clinic, Rochester, MN

Abstract

Long bones are formed and repaired through the process of endochondral ossification. Activation of G protein-coupled receptor (GPCR) signaling pathways is crucial for skeletal development and long bone growth. G protein-gated inwardly-rectifying K^+ (GIRK) channel genes are key functional components and effectors of GPCR signaling pathways in excitable cells of the heart and brain, but their roles in non-excitable cells that directly contribute to endochondral bone formation have not been studied. In this study, we analyzed skeletal phenotypes of *Girk2*$^{-/-}$, *Girk3*$^{-/-}$ and *Girk2/3*$^{-/-}$ mice. Bones from 12-week-old *Girk2*$^{-/-}$ mice were normal in length, but femurs and tibiae from *Girk3*$^{-/-}$ and *Girk2/3*$^{-/-}$ mice were longer than age-matched controls

Corresponding author: Jennifer J. Westendorf, Ph.D., Mayo Clinic, 200 First Street SW, Rochester, MN 55905, Phone: 507-538-5651, westendorf.jennifer@mayo.edu.

§Authors contributed equally

Author CRediT Statement

Earnest L. Taylor: Conceptualization, methodology, validation, formal analysis, investigation, writing-original draft, visualization
Samantha R. Weaver: Conceptualization, methodology, validation, formal analysis, investigation, writing-original draft, visualization
Ian M. Lorang: Investigation
Katherine M. Arnold: Methodology, investigation
Elizabeth W. Bradley: Conceptualization, methodology, formal analysis, investigation, writing-review and editing, visualization
Ezequiel Marron Fernandez de Velasco: Investigation, resources, writing-review and editing Kevin Wickman: Resources, writing-review and editing, project administration, funding acquisition
Jennifer J. Westendorf: Conceptualization, resources, writing-review and editing, supervision, project administration, funding acquisition

at 12-weeks-old. Epiphyseal chondrocytes from 5-day-old *Girk3*$^{-/-}$ mice expressed higher levels of genes involved in collagen chain trimerization and collagen fibril assembly, lower levels of genes encoding VEGF receptors, and produced larger micromasses than wildtype chondrocytes *in vitro*. *Girk3*$^{-/-}$ chondrocytes were also more responsive to the kappa opioid receptor (KOR) ligand dynorphin, as evidenced by greater pCREB expression, greater cAMP and GAG production, and upregulation of Col2a1 and Sox9 transcripts. Imaging studies showed that *Kdr (Vegfr2)* and endomucin expression was dramatically reduced in bones from young *Girk3*$^{-/-}$ mice, supporting a role for delayed vasculogenesis and extended postnatal endochondral bone growth. Together these data indicate that GIRK3 controls several processes involved in bone lengthening.

Keywords

cartilage; development; K^+ channel; GPCR; G protein; kappa opioid

1. INTRODUCTION

Long bones form and regenerate via endochondral ossification. During this process, mesenchymal stem cells in the limb bud condense and then differentiate into chondrocytes. Chondrocytes mature and spatially separate in the growth plate into proliferative, pre-hypertrophic, and hypertrophic zones, with the latter driving appositional long bone growth [1]. Vascular invasion of the cartilaginous matrix brings precursors for osteoclasts and osteoblasts that remodel and ossify the skeleton [2, 3]. Most hypertrophic chondrocytes will undergo apoptosis, but some survive, dedifferentiate, and find harbor in the bone marrow where they are poised to contribute to fracture repair and other processes in adults [4-6]. Many signaling and transcriptional pathways in chondrocytes orchestrate these dynamic and complex developmental processes, including ones driven by G protein-coupled receptors (GPCRs). Over 900 GPCRs are encoded by the human genome and many, including the kappa opioid receptor (KOR), are involved in skeletal development and repair [7-11]. In this study, we investigated the potential contribution of G protein-gated inwardly-rectifying K^+ (GIRK) channels – critical effectors of inhibitory G protein signaling in the heart and brain – in endochondral bone formation.

GIRK channels are homo- and hetero-tetramers formed by four mammalian GIRK subunits (GIRK1/*Kcnj3*, GIRK2/*Kcnj6*, GIRK3/*Kcnj9*, and GIRK4/*Kcnj5*) [12, 13]. GIRK channels are activated when GPCR ligands stimulate pertussis toxin-sensitive $G_{i/o}$-G proteins; the liberated $G\beta\gamma$ subunit then binds to GIRK channels and increases their gating [14-16]. The resultant efflux of K^+ reduces the excitability of neurons [12] and cardiomyocytes [17]. Knockout studies in mice have shown that GIRK2-containing GIRK channels mediate pain relief evoked by opioids and other analgesics [18-20]. In chondrocytes, K^+ efflux reduces swelling during unloading [21] and can affect proteoglycan secretion [22].

The four GIRK subunits share a high degree of homology, but distinct structural elements influence subcellular trafficking and channel regulation [12]. For example, GIRK2 and GIRK4 can form homo-tetramers [23, 24], but GIRK1 lacks an ER (endoplasmic reticulum) export domain and must form hetero-tetramers (*e.g.*, with GIRK2 in neurons or GIRK4

in cardiomyocytes) to be transported to the cell surface [25]. GIRK3 contains a lysosomal targeting sequence not found in other GIRK subunits [25]. Thus, while ectopic expression of GIRK1, GIRK2 or GIRK4 enhances channel activity, GIRK3 over-expression suppresses channel activity, likely promoting GIRK channel internalization [26-28]. GIRK3 also interacts with negative regulators of G protein signaling and lysosomal proteins [29, 30] to regulate intracellular trafficking of GIRK channels [31-33]. *In vivo*, GIRK3 is required for multiple forms of experience-induced plasticity of GIRK-dependent signaling [34, 35]. The distinct molecular and functional characteristics of GIRK3, including its role GIRK channel trafficking, position it as a potentially critical regulator of inhibitor GPCR-dependent signaling and GIRK channel function *in vivo*.

GIRK channels are effectors of GPCR signaling stimulated by a variety of agonists, including opioids [36-38]. Endogenous opioid peptides and their receptors are expressed in developing skeletons and contribute to long bone development [9, 39-41]. Kappa opioid receptors (KOR) and endogenous peptide ligands (e.g., dynorphin (Dyn)) enhance endochondral ossification and promote joint health [9, 10, 42]. Mice lacking genes for the kappa opioid receptor (*Oprk1*) or prodynorphin (*Pdyn*) have reduced bone density [9] and display accelerated articular cartilage degeneration after injury [10]. In chondrocytes, kappa opioids stimulate cAMP and pCREB activity and modulate Hedgehog signaling to protect articular cartilage after injury [9-11]. GIRK channels are downstream targets of opioid receptor activation in the brain and spinal cord [20, 43, 44], and have been implicated in some breast cancers [45, 46], but their roles in non-excitable cell types, including those that directly contribute to endochondral bone formation, have not been studied. This is despite evidence of *GIRK2* mutations in patients with Keppen Lubinsky syndrome, which is characterized by growth above the 50^{th} to 75^{th} percentile at birth with subsequent developmental delays and other phenotypes [47]. Here we report that *Girk2* deletion has no effect on femur and tibia length in C57BL/6J mice. In contrast, *Girk3* deletion increases femur and tibia lengths and augments kappa opioid signaling in chondrocytes. Thus, these data identify GIRK3 as a suppressor of bone lengthening and kappa opioid activity in developing skeletons.

2. METHODS

2.1 Mice

Generation of *Girk2*$^{-/-}$ and *Girk3*$^{-/-}$ mice was described previously [43, 48]. *Girk2*$^{-/-}$, *Girk3*$^{-/-}$, *Girk2/3*$^{-/-}$ and wildtype (WT) mice [48, 49] were maintained on the C57BL/6J background. In initial studies, *Girk2*$^{+/-}$ x *Girk3*$^{+/-}$ breeding pairs were established. However, offspring from these breeding pairs had low survival due to dermatitis and spontaneous seizures as previously documented in *Girk2*$^{-/-}$ mice [48, 50]. Therefore, *Girk2*$^{+/-}$ x *Girk2*$^{+/-}$ and *Girk3*$^{+/-}$ x *Girk3*$^{+/-}$ breeding pairs were established for additional studies. The Mayo Clinic Institutional Animal Care and Use Committee approved all experiments, and work was completed according to guidelines of the National Institutes of Health and the Institute of Laboratory Animal Resources, National Research Council. Animals were housed in an accredited facility with 12-hour light/dark cycles and supplied food and water *ad libitum* (Pico-Lab® Rodent Diet 20, LabDiet).

2.2 Longitudinal Measurements of Bone Length

Offspring from *Girk2*$^{+/-}$ x *Girk3*$^{+/-}$ breeding pairs generated WT, *Girk2*$^{-/-}$, *Girk3*$^{-/-}$, and *Girk2/3*$^{-/-}$ mice that were aged to 12-weeks-old. Femur and tibia lengths were determined post-mortem using x-ray images collected on a Faxitron Imager and ImageJ software [51]. A separate cohort of *Girk2*$^{+/-}$ x *Girk2*$^{+/-}$ breeding pairs yielded WT and *Girk2*$^{-/-}$ mice that were aged to 12-weeks-old, at which time femur and tibia lengths were determined post-mortem using x-ray images collected on a Faxitron Imager and ImageJ software. To study *Girk3*$^{-/-}$ mice, offspring of *Girk3*$^{+/-}$ x *Girk3*$^{+/-}$ breeding pairs were used. Femur and tibia lengths of male and female WT and *Girk3*$^{-/-}$ mice were measured weekly, from 3 weeks of age (post-weaning) until 12 weeks of age, with calipers. Femur lengths were also determined following x-ray and using ImageJ from separate cohorts of male mice that were aged to 4 weeks old for microcomputed tomography and dynamic histomorphometry, as well as 7-day-old female mice used for *in situ* hybridization.

2.3 Isolation and Culture of Immature Mouse Chondrocytes

Primary immature murine epiphyseal chondrocytes (IMCs) were collected from 5-day-old mice (P5) as previously described [52]. Briefly, IMCs were digested for one hour in 3 mg/mL collagenase, then overnight in 0.5 mg/mL collagenase in Dulbecco's modified Eagle's medium (DMEM) without fetal bovine serum (FBS) prior to seeding. For RNA-sequencing experiments and real-time quantitative PCR (QPCR) validation experiments, freshly isolated WT and *Girk3*$^{-/-}$ IMCs were washed with PBS and lysed as described below. For cAMP experiments, western blotting, and QPCR analyses, IMCs were plated in monolayer ($1x10^5$ cells per well in a six-well plate) in growth medium (DMEM with 10% FBS and 1% antibiotic/antimycotic). For GAG assays, IMCs were plated in micromasses at a density of $2x10^5$ cells per micromass in 35 mm petri dishes. Three micromasses were placed in each dish and cultured for three days in DMEM supplemented with 2% FBS and 1% antibiotic/antimycotic as previously described [52, 53]. The medium was switched to DMEM supplemented with 2% FBS, 1% antibiotic/antimycotic, 1x ITS (Insulin Transferrin Selenium; Gibco), 0.05 mg/ml ascorbic acid and 10 mM β-glycerophosphate to promote chondrogenesis. For kappa opioid agonist / antagonist experiments, Dynorphin (Dyn; Tocris 3195) (0.1 μM or 1 μM) or Norbinaltorphimine (Nor-B; Tocris 0347) (20 μM) were added to respective micromass or monolayer cultures for the indicated time periods with media changes every three days. For cells co-treated with both Dyn and Nor-B, Nor-B was applied two hours prior to Dyn.

2.4 RNA-sequencing (RNA-seq) and Pathway Analysis

RNA was isolated from IMCs from P5 WT and *Girk3*$^{-/-}$ mice (n=3 each). TruSeq RNA method was used for analysis of polyadenylated mRNAs that were selected using oligo dT magnetic beads. TruSeq Kits were used for indexing to permit multiplex sample loading on the flow cells of an Illumina HiSeq 2000 sequencer. Gene expression was normalized to one million reads and corrected for gene length (reads per kilobase per million mapped reads, RPKM). Pathway analysis was performed with the top 106 differentially regulated genes (≥ 2 fold change) against Reactome, version 70 [54, 55]. CREB binding sites were identified in

genes using a CREB target gene database [56]. Gene expression data were submitted to the Gene Expression Omnibus database (accession number GSE192933).

2.5 RNA Isolation, Reverse Transcription, and Real-Time Quantitative PCR

IMCs from WT and *Girk3*$^{-/-}$ mice were washed with PBS and mechanically disrupted using a cell scraper in 1 mL of TRIzol (Invitrogen). Total RNA was extracted using phenol/chloroform and 2 μg was reverse transcribed to cDNA with the iScript cDNA Synthesis Kit (Bio-Rad). QPCR was completed with the following gene-specific primers: *Col2a1, Col4a6, Col10a1, Girk3, Kdr, Oprk1, Pdyn, Sox9*, and *Vegfa* (Supplementary Table 1). Transcript levels were normalized to the reference gene *Ywhaz*. Abundance and relative fold changes in transcript gene expression were quantified using the $2^{-\Delta\Delta Ct}$ method relative to the control, vehicle-treated cultures at zero hours [57].

2.6 Western Blotting

WT or *Girk3*$^{-/-}$ IMCs were washed three times with ice-cold PBS, collected by centrifugation, and resuspended in cell lysis buffer (0.1% glycerol, 0.01% SDS, 0.1 M Tris, pH 6.8) with protease inhibitor mixture (Roche). Protein content was quantified using the DC™ protein assay (Bio-Rad) according to the manufacturer's protocol. Protein samples (30 μg) were resolved by SDS-PAGE and transferred to a polyvinylidene difluoride membrane. Western blotting was performed with primary antibodies at 1:1,000 dilution for GIRK3 (Alomone Labs APC-038), Actin (Sigma A4700), pCREB1 (pSer133, Cell Signaling 9198) and all CREB1 proteins (Cell Signaling 9197), followed by horse radish peroxidase (HRP)-conjugated goat anti-rabbit secondary antibodies at 1:10,000 dilution or goat anti-mouse secondaries at 1:1,000 dilution. Blots were incubated with SuperSignal Femto Chemiluminescent Substrate (Pierce) for 2 minutes and imaged on a GelDoc Go System (BioRad). Each experiment was repeated a minimum of three times. Blots from one representative experiment are shown.

2.8 Cell Proliferation Assays

WT or *Girk3*$^{-/-}$ IMCs (5 x 10^3 cells/well) were plated in monolayer in a 48-well plate and cultured overnight as previously described [58]. Cell confluency was detected in real-time with the IncuCyte S3 Live Cell Analysis System (Roche) with four captures per well every hour for 48 hours.

2.9 Alcian Blue Staining and Perichondrial Thickness Measurements

IMC micromasses were fixed with 10% neutral buffered formalin for 10 minutes and stained with 0.5% Alcian blue dye for 2 hours. Each experiment was performed in triplicate and repeated at least three times. Results from a representative experiment are shown. For Alcian blue staining of tissue sections, slides were deparaffinized, then incubated in 0.5% Alcian blue dye for 5 minutes followed by eosin counterstaining. Perichondrial thickness was evaluated in ImageJ by measuring three areas along the medial side of the proximal tibial growth plate in 4-week-old male mice on at least three sections per mouse.

2.10 Glycosaminoglycan (GAG) Assays

All IMC micromasses in a dish were digested overnight in a solution containing 0.05 M PBS, pH 6.5, 5 mM cysteine, 5 mM EDTA and 125 μg/ml papain. Samples were diluted 1:2 with digestion buffer to fit within the standard curve and added to a 96-well plate per the manufacturer's instructions (Chondrex 6022). Dye solution was applied to each well and plates were read at 525nm.

2.11 Cyclic AMP assays

Intracellular cAMP was determined using acid extraction and a commercial ELISA per the supplier's protocol (Cayman 581001). WT and *Girk3*$^{-/-}$ cells were plated at 1x10^5 cells per well in a 6-well plate and incubated with Dyn (1 μM) or Nor-B (20 μM). After 30 minutes, media were removed and 0.1 M HCl was added. Supernatant (50 μL) were diluted 1:2 to fit within the standard curve and plates were read at 420nm.

2.12 RNAScope In Situ Hybridization

Tibiae from 7-day-old WT and *Girk3*$^{-/-}$ mice were decalcified in EDTA for 2 to 3 days, embedded in paraffin, sectioned at 5 μm thickness, and secured to glass slides. *In situ* hybridization was performed using the RNAscope 2.5 HD Assay – BROWN (ACD Bio-techne 322300) per the manufacturer's instructions using probes targeted to *Kdr* (ACD Bio-techne 414811), *Flt1* (ACD Bio-techne 415541), *Mmp13* (ACD Bio-techne 482371), *Col2a1* (ACD Bio-techne 407221) and *Col10a1* (ACD Bio-techne 426181). Slides were imaged using a Zeiss LSM 900 confocal microscope. To quantify the number of positive cells, a 250 x 500 μm region of interest was drawn on the chondro-osseous border and number of punctate brown-stained nuclei were quantified by three independent reviewers.

2.13 Endomucin Immunofluorescence Staining

Tibiae from growing 3-week-old male mice were decalcified in EDTA for 10 days, embedded in paraffin, and sectioned. Specimens were incubated in blocking buffer (5% bovine serum albumin (BSA), 5% goat serum in Tris-Buffered Saline-Tween 20 (TBST)) for one hour at 25°C. Blocking buffer was replaced with the Endomucin (Santa Cruz, sc-65495 AF488) primary antibody solution (1:500 in blocking buffer) overnight at 4°C. Specimens were washed in PBS three times for 10 minutes each and then imaged using a Zeiss LSM 900 confocal microscope.

2.14 Microcomputed Tomography

Micro-CT imaging of the femur was performed using a SkyScan 1276 scanner (Bruker, Kontich, Belgium). Bones were fixed in 10% NBF before storage in 70% ethanol. Scans were performed at 55kV, 200 μA, 10 μm pixel resolution, 0.4° rotation steps for 360°, 4 frames average imaging with a 0.25mm A1 filter. The acquired scans were reconstructed using the Skyscan NRecon software with beam hardening and post-alignment correction. Trabecular and cortical analyses of the femur were performed using Bruker CtAN software. The datasets were oriented in 3D to vertically align the longitudinal axis of each femur. As the bones were different lengths, a region of interest (ROI) for trabecular bone was defined as 5% the length of each bone, beginning 10% bone's-length distance away from the distal

growth plate (Supp Fig 1A-1C). A gray-value threshold of 70 was applied to trabecular segmentations. Quantified outcomes were bone volume / total volume (BV/TV), trabecular thickness (TbTh), trabecular number (TbN), trabecular spacing (TbSp), and bone mineral density (BMD). For cortical bone analyses, the ROI was defined as 5% of total femur length beginning at the femoral midpoint (Supp Fig 1D-1F). Quantified outcomes for cortical bone were tissue mineral density (TMD), cortical thickness (CTh), and cortical bone area fraction (BAF) [59]. Bone width was evaluated at 5% bone-length's distance away from the distal femoral growth plate.

The growth plate thickness of the distal femur was reconstructed from microCT scans. Semi-automatic segmentation of the growth plate was performed using 3D Slicer and a 3D region-growing method [60, 61]. Bone was thresholded at the same value for all samples, and seeds were placed in the growth plate and the background on approximately 10 slices in both the coronal and sagittal planes. The "grow from seeds" feature was then applied to map the input image to user-specified segments, avoiding the already segmented bone. "Joint smoothing" was used on the resulting segmentation to preserve segment interfaces while removing noise. The growth plate segment was then exported as a 3D patch object to MatLab where the model was scaled appropriately and binarization performed to calculate its volume and peak cross sectional area [62]. Thickness measurements were taken by applying a query grid with 50 micron spacing and sampling the z values of the patch object at the query points, resulting in approximately 3,500 measurements across the growth plate. From these values, minimum, maximum, and mean thicknesses were calculated, and thickness distribution was plotted as a color map onto the patch object. Since the femoral growth plates had dramatic gradients across the surface, a small region of interest was taken in the center of each growth plate to establish a representative sample of growth plate thickness. Specifically, a 0.5mm diameter circle was selected on the 3D model and this core was exported separately. The same analysis was performed, resulting in approximately 100 thickness measurements in the ROI. Outliers were caused by measurement clipping the edge of the 3D model, not measuring the entire thickness. These values were removed, and mean thickness calculated.

2.15 Dynamic Histomorphometry

Four-week-old male WT (n=4) and *Girk3*$^{-/-}$ (n=4) mice received intraperitoneal calcein injections (10 mg/kg) 4 and 2 days prior to euthanasia to permit dynamic histomorphometry studies of bone remodeling as previously described [63, 64].

2.16 Statistics

Statistics were performed in Prism GraphPad (Version 9) using Student's t-test or two-way ANOVA as appropriate with post-hoc tests for multiple comparisons. Data are depicted as means or individual points with SD bars (n=3).

3. RESULTS

3.1 *Girk3*$^{-/-}$ mice have longer bones

Initial phenotypic analysis of a small number of littermates from *Girk2*$^{+/-}$ x *Girk3*$^{+/-}$ breeding pairs indicated that *Girk2/3*$^{-/-}$ and *Girk3*$^{-/-}$ mice had longer hind limbs than WT and *Girk2*$^{-/-}$ mice (Table 1; Fig 1A, 1B). However, breeding *Girk2*$^{+/-}$ x *Girk3*$^{+/-}$ mice was inefficient due to spontaneous seizures and dermatitis in the offspring [48, 50]. As such, initial results were validated in cohorts of *Girk2*$^{-/-}$ and *Girk3*$^{-/-}$ mice. *Girk2* deletion did not affect femur or tibia lengths in males and produced slightly smaller female mice (Table 1; Fig 1C, 1D). In contrast, *Girk3*$^{-/-}$ mice had longer femurs and tibiae than WT mice. In a longitudinal experiment, differences in bone length were observed in *Girk3*$^{-/-}$ mice from weaning (3 weeks of age) through 12 weeks of age in both male and female mice (Fig 1E, 1F). Femurs were 8% longer in male and female *Girk3*$^{-/-}$ mice than in WT mice. Tibiae were 10% and 8% longer, in male and female *Girk3*$^{-/-}$ mice, respectively. We next examined femur lengths of 1-week-old mice and did not observe any difference in length between WT and *Girk3*$^{-/-}$ mice (Supp Fig 2A, B). Histologic analysis of the growth plate cell dynamics at this age failed to reveal changes in the length of the growth plate or the hypertrophic zone, characterized by *Col10a1*-positive chondrocytes, or proliferative zone, characterized by *Col2a1*-positive chondrocytes, in *Girk3*$^{-/-}$ mice compared to WT mice (Supp Fig 2C, D).

Similarly, at 4 weeks of age, the overall growth plate thickness in the distal femur was not significantly different in *Girk3*$^{-/-}$ mice (Supp Fig 3).

No differences in femoral bone width, bone mineral density, bone formation rates, or polar moments of inertia were observed in 4-week-old *Girk3*$^{-/-}$ mice by microCT or histomorphometry (Table 2). These data demonstrate that germline deficiency of *Girk3*, but not *Girk2*, contributes to long bone growth. However, accelerated long bone growth in *Girk3*$^{-/-}$ mice is not directly attributable to a larger growth plate. Therefore, molecular experiments were next performed to gain understanding into the consequences of *Girk3* deletion on chondrocytes.

3.2 *Girk3* deletion induces genes associated with collagen assembly

RNA sequencing and bioinformatics analysis was performed on freshly isolated primary epiphyseal chondrocytes from P5 WT and *Girk3*$^{-/-}$ mice. We hypothesized that pathway analysis of these freshly isolated cells would identify mechanisms driving long bone growth. Reactome pathway analyses of genes upregulated by at least two-fold ($p<0.05$) in *Girk3*$^{-/-}$ chondrocytes (Fig 2A) identified pathways associated with laminin interactions, anchoring fiber formation, collagen trimerization and assembly, and extracellular matrix interactions (Table 3). Upregulated genes in these pathways included chondrocyte genes: *Chad, ChadI, Col4a6, Col23a1, Matn1/3* and *Col4a5* (Table 3). Additionally, *Alpl* was upregulated in *Girk3*$^{-/-}$ compared to WT chondrocytes (1.46-log2fold increase; p=3.77E-13). The differential expression of *Girk3* and several of these genes (*Col2a1, Col4a6, Col10a1, Sox9*) was confirmed by QPCR (Fig 2B, 2C). We therefore sought to characterize the effects of *Girk3* deletion on chondrocyte maturation.

3.3 *Girk3* deletion increases kappa-opioid signaling *in vitro*

Primary epiphyseal chondrocytes were isolated from P5 WT and *Girk3*$^{-/-}$ mice for *in vitro* studies (Fig 3A). *Girk3*$^{-/-}$ chondrocytes proliferated at the same rate as WT chondrocytes *in vitro* (Fig 3B). In micromass cultures, which are models of endochondral development, *Girk3*$^{-/-}$ chondrocytes produced more proteoglycans as detected qualitatively by Alcian blue staining after 6 days (Fig 3C, **top row**); however, secreted GAG concentrations in culture media were only modestly increased and not different statistically from WT cultures after three and six days (Fig 3D).

Bioinformatics analysis of the RNA-seq analysis revealed that the promoters for more than half (56%) of the differentially expressed genes in *Girk3*$^{-/-}$ chondrocytes contain binding elements for the transcription factor CREB1 [56]. CREB1 is phosphorylated by PKA and is shuttled to the nucleus in response to GPCR and G_s protein activation of adenylyl cyclases (AC) and rising cAMP levels. Basal levels of cAMP and pCREB1 were modestly higher in *Girk3*$^{-/-}$ than WT chondrocytes (Fig 4A, 4B), suggesting autocrine activation of these pathways in the absence of *Girk3*. Recent studies showed that kappa opioids activate pCREB and stimulate proteoglycan production in chondrocytes [10, 11]. RNA transcripts for *Oprk1* and *Pdyn* were elevated in *Girk3*$^{-/-}$ chondrocytes (Fig 2D). Thus, we next determined if adding the KOR agonist Dynorphin (Dyn) to cultures would affect cAMP and CREB activity differently in *Girk3*$^{-/-}$ compared to WT chondrocytes. Dyn increased cAMP levels (Fig 4A) and CREB phosphorylation (Fig 4B) in WT and *Girk3*$^{-/-}$ chondrocytes. Specifically, cAMP was higher in *Girk3*$^{-/-}$ cells exposed to Dyn than WT cells at 15 mins and pCREB1 was elevated in *Girk3*$^{-/-}$ cells exposed to Dyn at 45 minutes (Fig 4A, 4B). Dyn also increased GAG production (Fig 3D) and *Sox9* transcript levels (Fig 4D) in *Girk3*$^{-/-}$ chondrocytes. WT chondrocytes were also responsive to Dyn, as indicated by increased *Col2a1* and *Sox9* transcripts (Fig 4C, 4D). Norbinaltorphimine (Nor-B), a KOR antagonist, blocked the Dyn-induced responses of *Girk3*$^{-/-}$ and WT chondrocytes. Thus, *Girk3*$^{-/-}$ chondrocytes have greater autocrine Dyn signaling and display slightly higher basal cAMP signaling. They are also more responsive to GPCR stimulation by Dyn than WT chondrocytes *in vitro*.

3.4 *Girk3* ablation suppresses genes required for vascular invasion of the growth plate

Next, we examined down-regulated genes in *Girk3*$^{-/-}$ chondrocytes to better understand causative pathways for long bone growth in *Girk3*$^{-/-}$ mice. Several pathways downregulated in *Girk3*$^{-/-}$ chondrocytes focused on vascularization, with VEGF receptor and VEGF family genes (*Kdr, Flt1, Pgf*) identified as suppressed genes (Fig 2A; Table 4). Since vascularization of the growth plate is required for mineralization and remodeling of long bones during development [65] and *Flt1 (Vegfr1)* and *Kdr (Vegfr2)* are key receptors for VEGF in the skeleton [66], we assessed *Flt1* and *Kdr* expression and vascularization in *Girk3*$^{-/-}$ mice. Reductions in *Kdr* transcripts were confirmed in primary epiphyseal chondrocytes by QPCR (Fig 2E). *In situ, Kdr* was readily detected in the trabecular bone of WT mice but not *Girk3*$^{-/-}$ mice (Fig 5A); however, *Flt1* transcript levels were not different *in situ* (37.67 ± 17.02 in WT versus 35.67 ± 0.67 in *Girk3*$^{-/-}$ positive cells; p=0.9122; Fig 5B). *Vegfa* transcripts were not changed (Fig 2E). To confirm vascular suppression in *Girk3*$^{-/-}$ bones, endomucin was visualized by immunofluorescence in 3-week-old animals.

Endomucin is expressed in the vascular endothelial cells and is abundant in WT bone (Fig 5C). However, it was significantly reduced in the primary and secondary spongiosa of *Girk3*$^{-/-}$ tibiae. Vasculogenesis occurs following extracellular matrix remodeling and chondrocyte degradation at the chondro-osseous border. To assess chondrocyte degradation, Mmp13 levels were quantified via RNAScope. Mmp13 levels were higher at the chondro-osseous border in *Girk3*$^{-/-}$ mice (Fig 5D,E). These data suggest that delayed vascularization in *Girk3*$^{-/-}$ mice is associated with reductions in *Kdr* and endomucin expression. However, vascularization and intra-osseous remodeling still occur through the actions of Flt1 and Mmp13, respectively, in *Girk3*$^{-/-}$ mice.

4. DISCUSSION

Bone lengthening is governed by chondrocyte maturation and vascularization. Numerous GPCR-signaling pathways, including kappa opioids, influence growth. In this project, we assessed the role of critical effectors of inhibitory GPCRs in the heart and brain, the GIRK channels, on the maturation chondrocytes and bone length. GIRK channels are well-studied mediators of opioid responses in neurons, but their roles in non-excitable cell types that directly contribute to endochondral bone formation are not known. In this study, we found that the long bones of adolescent *Girk2*$^{-/-}$ mice were normal in length, while femurs and tibiae from *Girk3*$^{-/-}$ and *Girk2/3*$^{-/-}$ mice were longer. RNA sequencing and bioinformatic analysis demonstrated that chondrogenesis was enhanced in *Girk3*$^{-/-}$ chondrocytes even though no gross structural differences were observed in growth plates, perhaps indicating an increased rate of endochondral growth. *Girk3*$^{-/-}$ chondrocytes were more responsive to the KOR agonist, Dyn, as evidenced by greater cAMP and pCREB activity, greater GAG production, and upregulation of *Col2a1* and *Sox9* transcripts. Analysis of downregulated genes in *Girk3*$^{-/-}$ chondrocytes suggested that vascularization may be altered. Immunofluorescence studies showed that *Kdr* (*Vegfr2*) and endomucin were dramatically reduced in bones from young *Girk3*$^{-/-}$ mice, supporting a role for altered vasculogenesis during postnatal growth as one of likely many consequences of deleting *Girk3*.

Girk3$^{-/-}$ mice have longer tibiae and femurs than WT mice during postnatal growth. We did not observe significant changes in bone widths, perichondrium thickness, or the size/depth of growth plates in 4-week-old mice *Girk3*$^{-/-}$ mice. It is possible that the additive differences in both distal and proximal growth plates of the femur and/or tibia contribute to the significant length differences in *Girk3*$^{-/-}$ mice. Alternatively, it is possible that there is a systemic endocrinological or endogenous factor driving accelerated bone growth in *Girk3*$^{-/-}$ mice that is not chondrocyte autonomous or directly related to the size of the growth plate. Importantly, growth plate height measured at a single age (P7) is not necessarily reflective of the rate of growth. Future studies specifically designed to examine the rate of growth in *Girk3*$^{-/-}$ mice are warranted. RNA-seq data on primary epiphyseal chondrocytes demonstrates enhanced chondrogenic matrix production and markers of terminal differentiation such as *Alpl* and *Mmp13* in *Girk3*$^{-/-}$ mice compared to WT littermates. These data suggest that loss of GIRK3 primes chondrocytes for a short period of postnatal bone lengthening.

GIRK3 may control GPCR responses or other functions in chondrocytes. GIRK channels regulate the flow of K^+ ions out of the cell. Attempts to measure GIRK channel activity in chondrocytes, and the effect of GIRK3 deletion, were stymied by the low resting membrane potential of chondrocytes (data not shown). It is possible that GIRK3 has functions not associated with ion channel activity. GIRK3 is structurally and functionally different from GIRK1, GIRK2, and GIRK4. For example, GIRK3 contains a lysosomal targeting sequence that is not found in GIRK1, GIRK2 and GIRK4 [25]. Thus, while ectopic expression of GIRK1, GIRK2 or GIRK4 enhances channel activity, GIRK3 over-expression suppresses channel activity [27]. GIRK3 also interacts with negative regulators of G protein signaling (RGS2) [29] and sorting nexin 27 (SNX27) [30], to shuttle GIRK channels to the lysosome and down-regulate their expression [25, 31-33]. Identification of cellular pathways affected by GIRK3 in chondrocytes requires further investigation, but our data indicated that it may be required for fine-tuning GPCR responses, particularly KOR responses.

Kappa opioid receptors (KOR) and endogenous peptide ligands (e.g., dynorphin) contribute to endochondral ossification and joint health [9, 10, 42]. Genes for natural kappa opioid peptides (*Pdyn*, Dyn) and their receptors (*Oprk1*, KOR) are expressed in developing skeletons and contribute to endochondral ossification and joint health [9, 10, 39-42]. We observed upregulation of *Pdyn* and *Oprk1* transcripts in *Girk3*$^{-/-}$ chondrocytes. We also observed heightened responsiveness to endogenous kappa opioid agonists in *Girk3*$^{-/-}$ chondrocytes. Dynorphin stimulated cAMP, followed by CREB1 phosphorylation, to increase chondrogenic genes, including *Sox9*. These *in vitro* results suggest that *Girk3*$^{-/-}$ mice may be more attuned to endogenous kappa opioid signaling *in vivo*, accelerating bone lengthening.

In addition to enhanced responsiveness to kappa opioid signaling, *Girk3*$^{-/-}$ mice display altered vascularization *in vitro* and *in vivo*. Vascularization markers Kdr (Vegfr2) and endomucin were reduced in the bone and growth plate of young *Girk3*$^{-/-}$ mice, but Flt1 (Vegfr1) was not changed in situ. Delayed vascularization in the *Girk3*$^{-/-}$ mice may slow closure of the growth plate during periods of skeletal development. As such, the longer growth period may contribute to excessive bone lengthening in *Girk3*$^{-/-}$ mice. Higher levels of Mmp13 *in situ* suggest that the bones are poised for growth when appropriate signals such as dynorphin, are present. It is also possible that Vegfr1 is a more important receptor for vascularization at this step in *Girk3*$^{-/-}$ mice. Importantly, there were no effects of *Girk3* deletion on bone density or polar moments of inertia at 4 weeks of age. Therefore, the effects of delayed vascularization on the growth plate in *Girk3*$^{-/-}$ do not affect ossification during growth.

Deletion of *Girk3* delays vascularization and increases responsiveness to kappa opioid signaling in chondrocytes. Each of these mechanisms could contribute independently or together to drive long bone growth in *Girk3*$^{-/-}$ mice. However, an alternative and unexplored explanation for increased bone length in *Girk3*$^{-/-}$ mice lies in mechanisms independent of musculoskeletal cells. GIRK3 is most highly expressed throughout the adult rodent brain and central nervous system [12, 67] and is required for multiple forms of experience-induced plasticity of GIRK-dependent signaling in neurons [34, 35]. It is also known that innervation of developing skeletons occurs in concert with vascularization [66]. Thus, it is possible that

GIRK3 activity in neurons contributes to vascularization and bone lengthening. Investigation of bone lengths in mice where GIRK3 is specifically deleted in neurons is needed to provide additional insights into these physiological mechanisms.

5. CONCLUSIONS

In summary, GIRK3 was identified as a multi-faceted determinant of skeletal growth through regulation of vascularization and kappa opioid signaling. *Girk3*$^{-/-}$ mice have longer femurs and tibiae throughout development. Within chondrocytes, GIRK3 regulates chondrogenesis and fine-tunes kappa opioid receptor signaling. Given that GIRK channels are well-known effectors of inhibitory GPCR signaling in the heart and brain, GIRK3 may participate in other GPCR responses in chondrocytes as well. *In vivo*, GIRK3 deletion delays vascularization in long bones, potentially slowing closure of the growth plate and extending the growth period. Limitations of this study are that all kappa opioid experiments were performed *in vitro* and that developmental studies were limited to the postnatal period. Additional studies on the tissue-specific and intracellular activities of GIRK3 are needed to fully understand its contributions to skeletal development.

Supplementary Material

Refer to Web version on PubMed Central for supplementary material.

ACKNOWLEDGEMENTS

This work was supported by research and training grants from the National Institutes of Health to KW (DA034696 and AA027544) and JJW (AR074228, AR056950, DK07352, AR065397, AR072634), and Regenerative Medicine Minnesota.

7. REFERENCES

1. Kronenberg HM, Developmental regulation of the growth plate. Nature, 2003. 423(6937): p. 332–6. [PubMed: 12748651]
2. Hall BK and Miyake T, All for one and one for all: condensations and the initiation of skeletal development. Bioessays, 2000. 22(2): p. 138–47. [PubMed: 10655033]
3. Carpio LR and Westendorf JJ, Histone Deacetylases in Cartilage Homeostasis and Osteoarthritis. Curr Rheumatol Rep, 2016. 18(8): p. 52. [PubMed: 27402109]
4. Zhou X, et al. , Chondrocytes transdifferentiate into osteoblasts in endochondral bone during development, postnatal growth and fracture healing in mice. PLoS Genet, 2014. 10(12): p. e1004820. [PubMed: 25474590]
5. Aghajanian P and Mohan S, The art of building bone: emerging role of chondrocyte-to-osteoblast transdifferentiation in endochondral ossification. Bone Res, 2018. 6: p. 19. [PubMed: 29928541]
6. Yang L, et al. , Hypertrophic chondrocytes can become osteoblasts and osteocytes in endochondral bone formation. Proc Natl Acad Sci U S A, 2014. 111(33): p. 12097–102. [PubMed: 25092332]
7. Luo J, et al. , The role of GPCRs in bone diseases and dysfunctions. Bone Res, 2019. 7: p. 19. [PubMed: 31646011]
8. Law PY, Wong YH, and Loh HH, Molecular mechanisms and regulation of opioid receptor signaling. Annu Rev Pharmacol Toxicol, 2000. 40: p. 389–430. [PubMed: 10836142]
9. Baldock PA, et al. , The endogenous opioid dynorphin is required for normal bone homeostasis in mice. Neuropeptides, 2012. 46(6): p. 383–94. [PubMed: 23062312]
10. Wu L, et al. , Kappa opioid receptor signaling protects cartilage tissue against posttraumatic degeneration. JCI Insight, 2017. 2(1): p. e88553. [PubMed: 28097228]

11. Weber AE, et al. , Modulation of Hedgehog Signaling by Kappa Opioids to Attenuate Osteoarthritis. Arthritis Rheumatol, 2020. 72(8): p. 1278–1288. [PubMed: 32249508]
12. Lujan R, et al. , New insights into the therapeutic potential of Girk channels. Trends Neurosci, 2014. 37(1): p. 20–9. [PubMed: 24268819]
13. Lüscher C and Slesinger PA, Emerging roles for G protein-gated inwardly rectifying potassium (GIRK) channels in health and disease. Nat Rev Neurosci, 2010. 11(5): p. 301–15. [PubMed: 20389305]
14. Logothetis DE, et al. , The beta gamma subunits of GTP-binding proteins activate the muscarinic K+ channel in heart. Nature, 1987. 325(6102): p. 321–6. [PubMed: 2433589]
15. Wickman KD, et al. , Recombinant G-protein beta gamma-subunits activate the muscarinic-gated atrial potassium channel. Nature, 1994. 368(6468): p. 255–7. [PubMed: 8145826]
16. Krapivinsky G, et al. , G beta gamma binds directly to the G protein-gated K+ channel, IKACh. J Biol Chem, 1995. 270(49): p. 29059–62. [PubMed: 7493925]
17. Anderson A, et al. , Expression and relevance of the G protein-gated K(+) channel in the mouse ventricle. Sci Rep, 2018. 8(1): p. 1192. [PubMed: 29352184]
18. Blednov YA, et al. , A pervasive mechanism for analgesia: activation of GIRK2 channels. Proc Natl Acad Sci U S A, 2003. 100(1): p. 277–82. [PubMed: 12493843]
19. Mitrovic I, et al. , Contribution of GIRK2-mediated postsynaptic signaling to opiate and alpha 2-adrenergic analgesia and analgesic sex differences. Proc Natl Acad Sci U S A, 2003. 100(1): p. 271–6. [PubMed: 12496346]
20. Marker CL, Stoffel M, and Wickman K, Spinal G-protein-gated K+ channels formed by GIRK1 and GIRK2 subunits modulate thermal nociception and contribute to morphine analgesia. J Neurosci, 2004. 24(11): p. 2806–12. [PubMed: 15028774]
21. Lewis R, et al. , The role of the membrane potential in chondrocyte volume regulation. J Cell Physiol, 2011. 226(11): p. 2979–86. [PubMed: 21328349]
22. Barrett-Jolley R, et al. , The emerging chondrocyte channelome. Front Physiol, 2010. 1: p. 135. [PubMed: 21423376]
23. Dascal N, Signalling via the G protein-activated K+ channels. Cell Signal, 1997. 9(8): p. 551–73. [PubMed: 9429760]
24. Ferrer J, et al. , Pancreatic islet cells express a family of inwardly rectifying K+ channel subunits which interact to form G-protein-activated channels. J Biol Chem, 1995. 270(44): p. 26086–91. [PubMed: 7592809]
25. Ma D, et al. , Diverse trafficking patterns due to multiple traffic motifs in G protein-activated inwardly rectifying potassium channels from brain and heart. Neuron, 2002. 33(5): p. 715–29. [PubMed: 11879649]
26. Jelacic TM, et al. , Functional and biochemical evidence for G-protein-gated inwardly rectifying K+ (GIRK) channels composed of GIRK2 and GIRK3. J Biol Chem, 2000. 275(46): p. 36211–6. [PubMed: 10956667]
27. McCall NM, Marron E de Velasco Fernandez, and Wickman K, GIRK Channel Activity in Dopamine Neurons of the Ventral Tegmental Area Bidirectionally Regulates Behavioral Sensitivity to Cocaine. The Journal of Neuroscience, 2019. 39(19): p. 3600–3610. [PubMed: 30837265]
28. Kofuji P, Davidson N, and Lester HA, Evidence that neuronal G-protein-gated inwardly rectifying K+ channels are activated by G beta gamma subunits and function as heteromultimers. Proc Natl Acad Sci U S A, 1995. 92(14): p. 6542–6. [PubMed: 7604029]
29. Labouèbe G, et al. , RGS2 modulates coupling between GABAB receptors and GIRK channels in dopamine neurons of the ventral tegmental area. Nat Neurosci, 2007. 10(12): p. 1559–68. [PubMed: 17965710]
30. Lunn ML, et al. , A unique sorting nexin regulates trafficking of potassium channels via a PDZ domain interaction. Nat Neurosci, 2007. 10(10): p. 1249–59. [PubMed: 17828261]
31. Balana B, et al. , Ras-association domain of sorting Nexin 27 is critical for regulating expression of GIRK potassium channels. PLoS One, 2013. 8(3): p. e59800. [PubMed: 23536889]

32. Balana B, et al. , Mechanism underlying selective regulation of G protein-gated inwardly rectifying potassium channels by the psychostimulant-sensitive sorting nexin 27. Proc Natl Acad Sci U S A, 2011. 108(14): p. 5831–6. [PubMed: 21422294]
33. Munoz MB and Slesinger PA, Sorting nexin 27 regulation of G protein-gated inwardly rectifying K(+) channels attenuates in vivo cocaine response. Neuron, 2014. 82(3): p. 659–69. [PubMed: 24811384]
34. Lalive AL, et al. , Firing modes of dopamine neurons drive bidirectional GIRK channel plasticity. J Neurosci, 2014. 34(15): p. 5107–14. [PubMed: 24719090]
35. Munoz MB, et al. , A Role for the GIRK3 Subunit in Methamphetamine-Induced Attenuation of GABAB Receptor-Activated GIRK Currents in VTA Dopamine Neurons. J Neurosci, 2016. 36(11): p. 3106–14. [PubMed: 26985023]
36. Nagi K and Pineyro G, Kir3 channel signaling complexes: focus on opioid receptor signaling. Frontiers in Cellular Neuroscience, 2014. 8: p. 186. [PubMed: 25071446]
37. Ikeda K, et al. , Involvement of G-protein-activated inwardly rectifying K (GIRK) channels in opioid-induced analgesia. Neurosci Res, 2000. 38(1): p. 113–6. [PubMed: 10997585]
38. Ikeda K, et al., Opioid Receptor Coupling to GIRK Channels, in Opioid Research: Methods and Protocols, Pan ZZ, Editor. 2003, Humana Press: Totowa, NJ. p. 53–64.
39. Bohm M and Grassel S, Role of proopiomelanocortin-derived peptides and their receptors in the osteoarticular system: from basic to translational research. Endocr Rev, 2012. 33(4): p. 623–51. [PubMed: 22736674]
40. Spetea M, Opioid receptors and their ligands in the musculoskeletal system and relevance for pain control. Curr Pharm Des, 2013. 19(42): p. 7382–90. [PubMed: 23448480]
41. Perez-Castrillon JL, et al. , Expression of opioid receptors in osteoblast-like MG-63 cells, and effects of different opioid agonists on alkaline phosphatase and osteocalcin secretion by these cells. Neuroendocrinology, 2000. 72(3): p. 187–94. [PubMed: 11025413]
42. Bu G, et al. , Opioid Peptides and Their Receptors in Chickens: Structure, Functionality, and Tissue Distribution. Peptides, 2020. 128: p. 170307. [PubMed: 32217145]
43. Torrecilla M, et al. , G-protein-gated potassium channels containing Kir3.2 and Kir3.3 subunits mediate the acute inhibitory effects of opioids on locus ceruleus neurons. J Neurosci, 2002. 22(11): p. 4328–34. [PubMed: 12040038]
44. Kotecki L, et al. , GIRK Channels Modulate Opioid-Induced Motor Activity in a Cell Type- and Subunit-Dependent Manner. J Neurosci, 2015. 35(18): p. 7131–42. [PubMed: 25948263]
45. Dhar MS and Plummer HK 3rd, Protein expression of G-protein inwardly rectifying potassium channels (GIRK) in breast cancer cells. BMC Physiol, 2006. 6: p. 8. [PubMed: 16945134]
46. Rezania S, et al. , Overexpression of KCNJ3 gene splice variants affects vital parameters of the malignant breast cancer cell line MCF-7 in an opposing manner. BMC Cancer, 2016. 16: p. 628. [PubMed: 27519272]
47. Masotti A, et al. , Keppen-Lubinsky syndrome is caused by mutations in the inwardly rectifying K+ channel encoded by KCNJ6. Am J Hum Genet, 2015. 96(2): p. 295–300. [PubMed: 25620207]
48. Signorini S, et al. , Normal cerebellar development but susceptibility to seizures in mice lacking G protein-coupled, inwardly rectifying K+ channel GIRK2. Proc Natl Acad Sci U S A, 1997. 94(3): p. 923–7. [PubMed: 9023358]
49. Belzung C and Griebel G, Measuring normal and pathological anxiety-like behaviour in mice: a review. Behav Brain Res, 2001. 125(1-2): p. 141–9. [PubMed: 11682105]
50. Hallmann K, et al. , Mutation analysis of the inwardly rectifying K(+) channels KCNJ6 (GIRK2) and KCNJ3 (GIRK1) in juvenile myoclonic epilepsy. Am J Med Genet, 2000. 96(1): p. 8–11. [PubMed: 10686544]
51. Schneider CA, Rasband WS, and Eliceiri KW, NIH Image to ImageJ: 25 years of image analysis. Nature Methods, 2012. 9(7): p. 671–675. [PubMed: 22930834]
52. Gosset M, et al. , Primary culture and phenotyping of murine chondrocytes. Nat Protoc, 2008. 3(8): p. 1253–60. [PubMed: 18714293]
53. Bradley EW, et al. , Deletion of the PH-domain and Leucine-rich Repeat Protein Phosphatase 1 (Phlpp1) Increases Fibroblast Growth Factor (Fgf) 18 Expression and Promotes Chondrocyte Proliferation. J Biol Chem, 2015. 290(26): p. 16272–80. [PubMed: 25953896]

54. Fabregat A, et al. , The Reactome pathway Knowledgebase. Nucleic Acids Res, 2016. 44(D1): p. D481–7. [PubMed: 26656494]
55. Fabregat A, et al. , Reactome pathway analysis: a high-performance in-memory approach. BMC Bioinformatics, 2017. 18(1): p. 142. [PubMed: 28249561]
56. Zhang X, et al. , Genome-wide analysis of cAMP-response element binding protein occupancy, phosphorylation, and target gene activation in human tissues. Proc Natl Acad Sci U S A, 2005. 102(12): p. 4459–64. [PubMed: 15753290]
57. Livak KJ and Schmittgen TD, Analysis of relative gene expression data using real-time quantitative PCR and the 2(-Delta Delta C(T)) Method. Methods, 2001. 25(4): p. 402–8. [PubMed: 11846609]
58. Weaver SR, et al. , Pleckstrin homology (PH) domain and Leucine Rich Repeat Phosphatase 1 (Phlpp1) Suppresses Parathyroid Hormone Receptor 1 (Pth1r) Expression and Signaling During Bone Growth. Journal of Bone and Mineral Research, 2021. 36(5): p. 986–999. [PubMed: 33434347]
59. Bouxsein ML, et al. , Guidelines for assessment of bone microstructure in rodents using micro-computed tomography. J Bone Miner Res, 2010. 25(7): p. 1468–86. [PubMed: 20533309]
60. Fedorov A, et al. , 3D Slicer as an image computing platform for the Quantitative Imaging Network. Magn Reson Imaging, 2012. 30(9): p. 1323–41. [PubMed: 22770690]
61. Weaver SR, et al. , Pleckstrin homology (PH) domain and Leucine Rich Repeat Phosphatase 1 (Phlpp1) Suppresses Parathyroid Hormone Receptor 1 (Pth1r) Expression and Signaling During Bone Growth. Journal of Bone and Mineral Research. **n/a**(n/a).**n/a**
62. Aitkenhead A, Mesh Voxelization. 2020, Mathworks: MatLab Central File Exchange.
63. McGee-Lawrence ME, et al. , Histone deacetylase 3 is required for maintenance of bone mass during aging. Bone, 2013. 52(1): p. 296–307. [PubMed: 23085085]
64. Razidlo DF, et al. , Histone deacetylase 3 depletion in osteo/chondroprogenitor cells decreases bone density and increases marrow fat. PLoS One, 2010. 5(7): p. e11492. [PubMed: 20628553]
65. Sivaraj KK and Adams RH, Blood vessel formation and function in bone. Development, 2016. 143(15): p. 2706–15. [PubMed: 27486231]
66. Takahashi H and Shibuya M, The vascular endothelial growth factor (VEGF)/VEGF receptor system and its role under physiological and pathological conditions. Clin Sci (Lond), 2005. 109(3): p. 227–41. [PubMed: 16104843]
67. Karschin C, et al. , IRK(1–3) and GIRK(1–4) Inwardly Rectifying K^+Channel mRNAs Are Differentially Expressed in the Adult Rat Brain. The Journal of Neuroscience, 1996. 16(11): p. 3559–3570. [PubMed: 8642402]

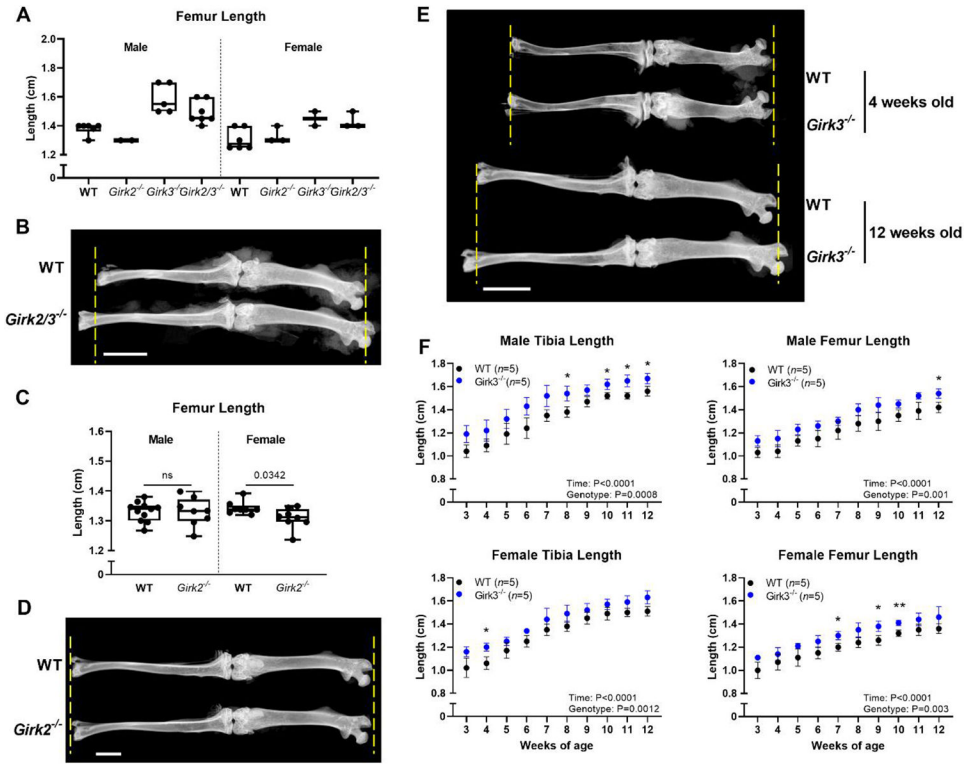

Figure 1. *Girk3*$^{-/-}$ mice have longer femora and tibiae than WT mice.

(**A**) Femur lengths of male and female WT, *Girk2*$^{-/-}$, *Girk3*$^{-/-}$, and *Girk2/3*$^{-/-}$ mice were measured at 12 weeks of age following dissection and x-ray. (**B**) X-rays of WT and *Girk2/3*$^{-/-}$ male mice at 12 weeks of age. Yellow dashed lines indicate the WT bone length. Scale bar indicates 5 mm. (**C**) Femur lengths of male and female WT and *Girk2*$^{-/-}$ mice were measured at 12 weeks of age following dissection and x-ray. Statistics were performed using Student's T-test. (**D**) X-rays of WT and *Girk2*$^{-/-}$ female mice at 12 weeks of age. Yellow dashed lines indicate the WT bone length. Scale bar indicates 2.5 mm. (**E**) X-rays of WT and *Girk3*$^{-/-}$ male mice at 4 weeks and 12 weeks of age. Yellow dashed lines indicate the WT bone length at each respective age. Scale bar indicates 5 mm. (**F**) Post-weaning growth rates of male femurs and tibiae from WT and *Girk3*$^{-/-}$ male and female mice. Bone lengths were determined using calipers. Statistics were performed using a two-way ANOVA with repeated measures. * : P<0.05, ** : P<0.01

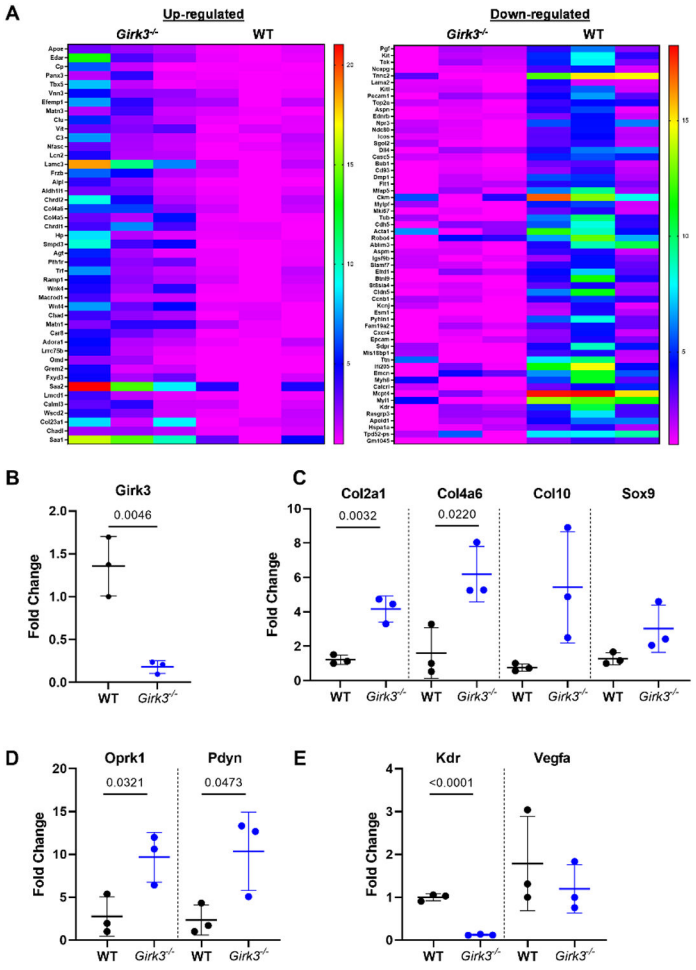

Figure 2. *Girk3* deletion alters the chondro-transcriptome.

(**A**) Heat maps of differentially regulated genes in *Girk3*$^{-/-}$ versus WT chondrocytes. RNA was collected from freshly isolated epiphyseal chondrocytes and prepared for bulk RNA-Seq. Semi-quantitative PCR of (**B**) *Girk3*, (**C**) *Col2a1, Col4a6, Col10a1, Sox9*, (**D**) *Oprk1, Pdyn*, (**E**) *Kdr*, and *Vegfa* was performed on freshly isolated chondrocytes from independent populations of WT and *Girk3*$^{-/-}$ mice. Statistics were performed using Student's T-test.

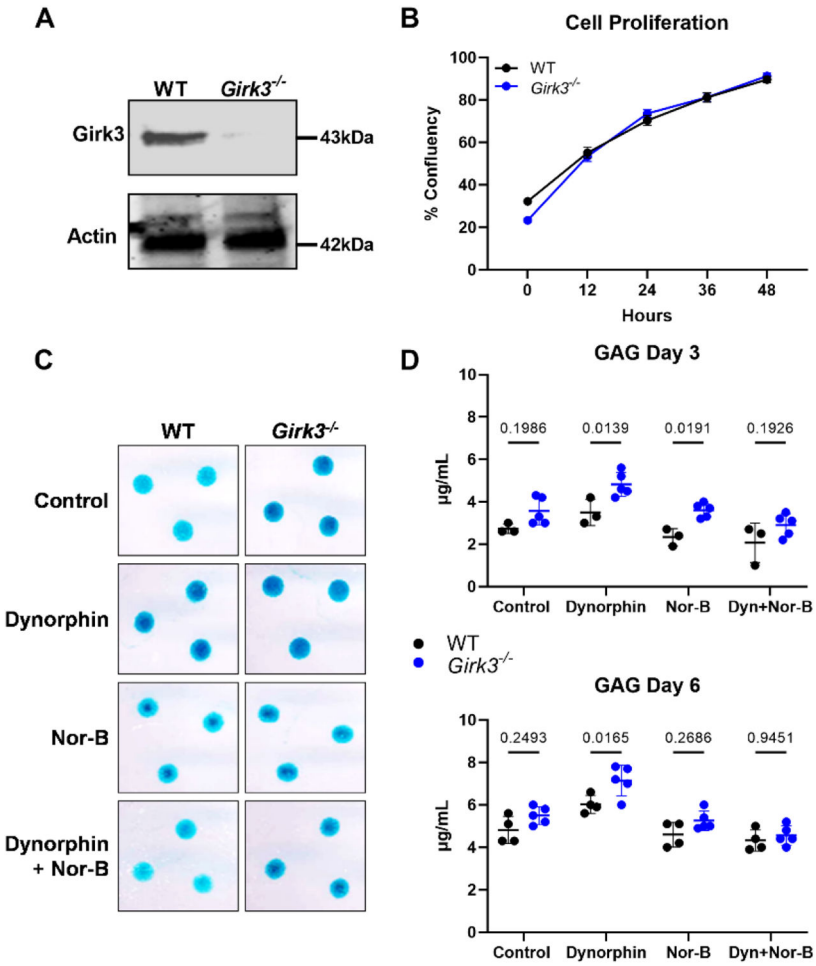

Figure 3. *Girk3* deletion increases kappa opioid-induced extracellular matrix production in chondrocyte cultures.

(**A**) GIRK3 and Actin were measured in cell lysates prepared from freshly isolated epiphyseal chondrocytes of WT and *Girk3*$^{-/-}$ mice via Western blotting. (**B**) Live cell imaging was performed over 48 hours on WT and *Girk3*$^{-/-}$ IMCs plated in monolayer and cell proliferation was determined based off cell confluency. (**C**) Alcian Blue staining showing matrix production by WT and *Girk3*$^{-/-}$ micromasses in response to Dynorphin (Dyn; 0.1µM) with or without Norbinaltorphimine (Nor-B; 20µM) after 6 days. (**D, E**) Glycosaminoglycan (GAG) production was measured in micromasses after (**C**) 3 and (**D**) 6 days in the indicated conditions. Statistics were performed using a two-way ANOVA.

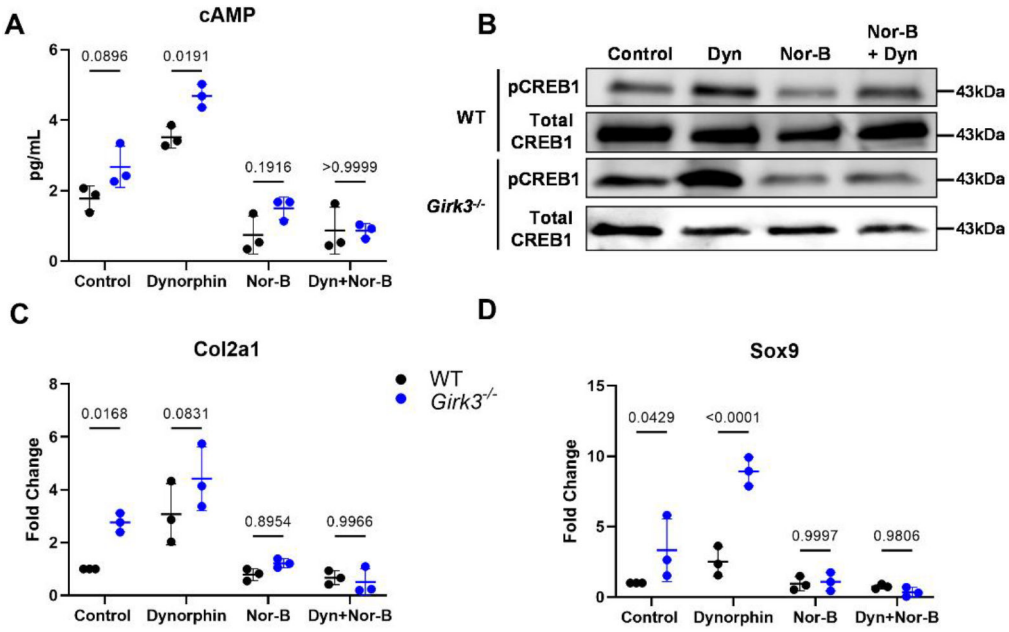

Figure 4. *Girk3* deletion increases kappa opioid induced CREB activation in chondrocyte cultures.

WT or *Girk3*$^{-/-}$ IMCs were cultured in monolayer in the presence of vehicle, Dyn and/or Nor-B. (**A**) Cyclic AMP production in the supernatant was measured via ELISA 15 min after 1μM Dyn and/or 20μM Nor-B were added to the culture. (**B**) pCREB1 and total CREB1 production were measured in cell lysates 45 minutes after 1μM Dyn and/or 20μM Nor-B were added. (**C, D**) QPCR was performed to measure expression levels of (**C**) *Col2a1* and (**D**) *Sox9* after 6 days in culture with 0.1μM Dyn and/or 20μM Nor-B. Statistics were performed using a two-way ANOVA.

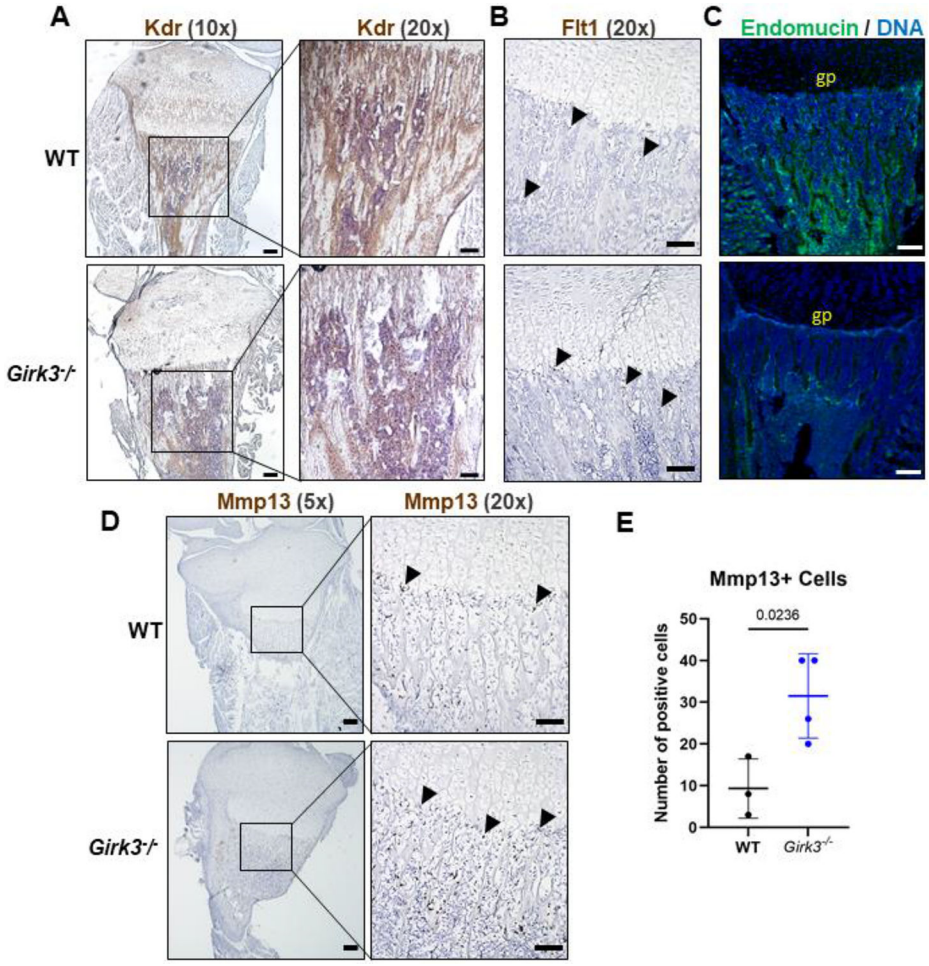

Figure 5. Vascularization of the primary spongiosa is reduced in *Girk3*$^{-/-}$ mice.

(**A-B**) RNAScope *in situ* hybridization was performed using probes targeted to Kdr and Flt1 on 1-week-old male WT and *Girk3*$^{-/-}$ mice. Images were taken at 10x (scale bar = 50 μm) or 20x (scale bar = 100 μm) to visualize positive brown staining in the primary spongiosa. (**C**) Maximum intensity projection of confocal images showing Endomucin (green) and DNA (DAPI, blue) in 3-week-old male WT and *Girk3*$^{-/-}$ mice. Scale bar indicates 100 μm. "gp" = growth plate. (**D,E**) RNAScope *in situ* hybridization was performed using a probe targeted to Mmp13 on 1-week-old male WT and *Girk3*$^{-/-}$ mice. Images were taken at 5x (scale bar = 50 μm) or 20x (scale bar = 100 μm) to visualize positive brown staining. (**E**) Number of Mmp13-positive brown stained cells (Mmp13+) were quantified along the chondro-osseous border.

Table 1.

Hind limbs are longer in 12-week-old *Girk2/3*$^{-/-}$, but not *Girk2*$^{-/-}$, mice

Parameter	**Length, cm (SD)**			
***Girk2/3*$^{-/-}$ Cohort**				
Males	**WT (*n*=6)**	***Girk2*$^{-/-}$ (*n*=2)**	***Girk3*$^{-/-}$ (*n*=5)**	***Girk2/3*$^{-/-}$ (*n*=7)**
Femur Length	1.38 (0.04)	1.3 (0)	1.59 (0.10)	1.49 (0.08)
Tibia Length	1.5 (0.06)	1.5 (0)	1.74 (0.11)	1.56 (0.12)
Females	**WT (*n*=6)**	***Girk2*$^{-/-}$ (*n*=3)**	***Girk3*$^{-/-}$ (*n*=2)**	***Girk2/3*$^{-/-}$ (*n*=3)**
Femur Length	1.31 (0.07)	1.33 (0.06)	1.45 (0.07)	1.43 (0.06)
Tibia Length	1.42 (0.12)	1.38 (0.10)	1.6 (0.14)	1.5 (0)
***Girk2*$^{-/-}$ Cohort**				
Males	**WT (*n*=11)**	***Girk2*$^{-/-}$ (*n*=8)**	**p-value**	
Femur Length	1.33 (0.03)	1.33 (0.05)	0.9767	
Tibia Length	1.66 (0.04)	1.67 (0.04)	0.8223	
Females	**WT (*n*=8)**	***Girk2*$^{-/-}$ (*n*=8)**	**p-value**	
Femur Length	1.34 (0.02)	1.31 (0.04)	0.0342	
Tibia Length	1.66 (0.03)	1.62 (0.04)	0.0505	

Table 2.

Bone parameters are normal in 4-week-old male *Girk3*$^{-/-}$ mice

Parameter	WT (SD)	*Girk3*$^{-/-}$ (SD)	p-value
MicroCT	**n=5**	**n=7**	
Length, mm	10.80 (0.15)	10.93 (0.18)	0.2150
Width, mm	2.56 (0.05)	2.58 (0.04)	0.5075
BV/TV, %	6.54 (2.65)	4.95 (1.60)	0.2228
BMD, gHA/cm^3	0.33 (0.01)	0.34 (0.01)	0.1577
Tb.Th, μm	54.81 (3.45)	59.56 (3.86)	0.0535
Tb.Sp, μm	301.4 (39.52)	346.4 (46.55)	0.1103
Tb.N, n/mm	1.18 (0.43)	0.82 (0.23)	0.0853
Ct.BAr, mm^2	0.51 (0.04)	0.52 (0.03	0.5660
Ct.TAr, mm^2	1.40 (0.09)	1.41 (0.08)	0.8192
Ct.BAF, %	36.59 (0.45)	37.15 (0.97)	0.2562
Ct.Th, mm	126.7 (4.96)	129.6 (5.15)	0.3472
Ct.TMD, gHA/cm^3	0.842 (0.029)	0.845 (0.014)	0.8480
Polar MOI, mm^4	0.188 (0.03)	0.193 (0.02)	0.7223
Histomorphometry	**n=4**	**n=4**	
OV/BV, %	4.73 (2.38)	3.27 (1.34)	0.3267
Tb.Th, μm	34.47 (5.53)	32.28 (4.36)	0.5570
Tb.Sp, μm	539.9 (271.2)	449.2 (127.1)	0.5674
Tb.N, n/mm	2.22 (1.42)	2.18 (0.52)	0.9607
LS/BS, %	28.37 (6.11)	33.30 (7.80)	0.3582
MAR, μm/day	4.28 (0.14)	3.93 (0.97)	0.4934
BFR/BS, μm^3/μm^2	1.22 (0.28)	1.29 (0.32)	0.7420
Ob.S/BS, %	35.90 (10.61)	35.11 (9.08)	0.9136
Oc.S/BS, %	11.84 (3.45)	9.52 (4.69)	0.4558

Table 3.

Pathways enriched by Genes Upregulated in *Girk3*$^{-/-}$ chondrocytes

Reactome Pathway	p-value	FDR	DEGs in Pathway
Laminin interactions	1.77e-07	9.18e-05	*Col23a1, Col4a5, Col4a6, Lamc3*
Anchoring fiber formation	3.45e-07	9.18e-05	*Col23a1, Col4a5, Col4a6*
Collagen chain trimerization	7.22e-07	1.28e-04	*Col23a1, Col4a5, Col4a6*
Crosslinking of collagen fibrils	2.21e-06	2.93e-04	*Col23a1, Col4a5, Col4a6*
Posttranslational protein phosphorylation	3.48e-06	3.69e-04	*Apoe, C3, Chrdl1, Cp, Matn3, Trf*
ECM proteoglycans	5.46e-06	4.80e-04	*Col23a1, Col4a5, Col4a6, Matn1, Matn3*
Collagen degradation	1.01e-05	7.70e-04	*Col23a1, Col4a5, Col4a6*
Collagen biosynthesis and modifying enzymes	5.84e-05	0.004	*Col23a1, Col4a5, Col4a6*
Regulation of IGF transport and uptake by IGFBPs	2.02e-04	0.012	*Apoe, C3, Chrdl1, Cp, Matn3, Trf*
Assembly of collagen fibrils and other multimeric structures	2.22e-04	0.012	*Col23a1, Col4a5, Col4a6*

Table 4.

Pathways affected by Genes Downregulated in *Girk3*$^{-/-}$ chondrocytes

Reactome Pathway	p-value	FDR	DEGs in Pathway
Attenuation phase	1.45e-09	8.99e-07	*Hspa1a*
HSF1-dependent transactivation	6.65e-09	2.06e-06	*Hspa1a*
Striated muscle contraction	1.07e-06	2.21e-04	*Acta1, Myh8, Myl1, Tnnc2, Ttn*
HSF1 activation	1.66e-05	0.003	*Hspa1a*
Regulation of HSF1-mediated heat shock response	6.54e-05	0.008	*Hspa1a, Bub1, Ablim3*
Cellular response to heat stress	1.50e-04	0.015	*Hspa1a, Bub1, Ablim3*
VEGF ligand-receptor interactions	2.21e-04	0.017	*Flt1, Kdr, Pgf*
VEGF binds to VEGFR leading to receptor dimerization	2.21e-04	0.017	*Flt1, Kdr, Pgf*